Graphene-Armored Aluminum Foil with Enhanced Anticorrosion Performance as Current Collectors for Lithium-Ion Battery

Mingzhan Wang, Miao Tang, Shulin Chen, Haina Ci, Kexin Wang, Liurong Shi, Li Lin, Huaying Ren, Jingyuan Shan, Peng Gao, Zhongfan Liu, and Hailin Peng**

Aluminum (Al) foil, as the most accepted cathode current collector for lithium-ion batteries (LIBs), is susceptible to local anodic corrosions during long-term operations. Such corrosions could lead to the deterioration or even premature failure of the batteries and are generally believed to be a bottleneck for next-generation 5 V LIBs. Here, it is demonstrated that Al foil armored by conformal graphene coating exhibits significantly reinforced anodic corrosion resistance in both $LiPF_6$ and lithium bis(trifluoromethanesulphonyl) imide (LiTFSI) based electrolytes. Moreover, $LiMn_2O_4$ cells using graphene-armored Al foil as current collectors (LMO/GA) demonstrate enhanced electrochemical performance in comparison with those using pristine Al foil (LMO/PA). The long-term discharge capacity retention of LMO/GA cell after ≈950 h straight operations at low rate (0.5 C) reaches up to 91%, remarkably superior to LMO/PA cell (75%). The self-discharge propensity of LMO/GA is clearly relieved and the rate/power performance is also improved with graphene mediations. This work not only contributes to the long-term stable operations of LIBs but also might catalyze the deployment of 5 V LIBs in the future.

M. Wang, M. Tang, S. Chen, H. Ci, K. Wang, L. Shi, Dr. L. Lin, H. Ren, J. Shan, Prof. P. Gao, Prof. Z. Liu, Prof. H. Peng
Center for Nanochemistry
Beijing Science and Engineering Center for Nanocarbons
Beijing National Laboratory for Molecular Sciences
College of Chemistry and Molecular Engineering
Peking University
Beijing 100871, P. R. China
E-mail: zfliu@pku.edu.cn; hlpeng@pku.edu.cn

S. Chen, Prof. P. Gao
Electron Microscopy Laboratory
and International Centre for Quantum Materials
School of Physics
Peking University
Beijing 100871, P. R. China

S. Chen
State Key Laboratory of Advanced Welding and Joining
Harbin Institute of Technology
Harbin 150001, P. R. China

H. Ci, H. Ren, J. Shan
Academy for Advanced Interdisciplinary Studies
Peking University
Beijing 100871, P. R. China

Prof. Z. Liu, Prof. H. Peng
Beijing Graphene Institute (BGI)
Beijing 100094, P. R. China

DOI: 10.1002/adma.201703882

Current collectors are essential components in rechargeable lithium-ion batteries (LIBs), whose primary tasks are to efficiently bridge the internal and external circuits.[1,2] Regardless of multifarious electrode materials, aluminum (Al) foil and copper (Cu) foil are the most well-established current collectors for positive and negative electrode materials in LIBs, respectively, probably due to their high electric conductivity, moderate chemical and electrochemical stability, and more importantly, low cost, etc.[3] However, both Al foil and Cu foil are susceptible to localized corrosions during long-term cycling.[4–9] Serious consequences can be readily perceived, including the increase of resistance, electric isolations of the active materials, the microshort-circuits induced by resultant Al/Cu fragments, the undesired parasitic side reactions, etc.[7,10] Therefore, the corrosions of Al/Cu foil are widely recognized as a nontrivial factor contributing to the degradation/failure of battery performance and reduced service life.[6,11] Strikingly, the anodic corrosions of Al foil are particularly prominent, considering the thermodynamic standard electrode potential of Al^{3+}/Al (1.38 V vs Li^+/Li) is much below the normal operating potential of most positive electrode.[8] As a result, the corrosions of Al foil not only deteriorate the long-term performances of current 4 V LIBs but also are generally believed to be a bottleneck for next-generation 5 V LIBs.

According to the well-defined model of the anodic corrosion of Al foil in organic electrolytes, the corrosion process is composed of consecutive elementary steps.[8,12,13]

First, driven by electrochemical force, the formation of Al^{3+} takes place

$$\text{Aluminum oxide} \rightarrow Al^{3+}_{(ad)} + O_2(g) + e^- \quad (1)$$

$$Al \rightarrow Al^{3+}_{(ad)} + 3e^- \quad (2)$$

Then, the unstable Al^{3+} (strong Lewis acid) tends to be coordinated or solvated to form complexes adsorbing on the surface with the participation of anion or solvent molecules

$$Al^{3+}_{(ad)} + \text{anion/solvent} \rightarrow \text{Al-complexes}_{(ad)} \quad (3)$$

Finally, the complexes adsorbing on the surface diffuse into the bulk electrolyte solution

$$\text{Al-complexes}_{(ad)} \rightarrow \text{Al-complexes}_{(sol)} \quad (4)$$

Obviously, according to this scenario, the corrosions of Al foil are induced by complicated and interdependent factors, including the applied anodic voltage,[5] the composition of the electrolyte,[7,8] the integrity and uniformity of the native oxide passive layer,[7] and even the coverage of the active material,[6] etc.

Particularly, the protecting effects of native oxide layer on the anodic corrosion of Al foil are useful rather subtle. On one hand, the native oxide layer efficaciously overcomes the unfavorable thermodynamic factor and endows kinetic stability to Al foil as cathode current collector.[8] However, such protecting effects turn out to be fairly subtle and particularly dependent upon the electrolyte composition, presumably due to the kinetic nature.[6,8]

For example, $LiPF_6$-based electrolyte, the state-of-the-art and benchmark electrolyte for LIBs imparted with best trade-off electrochemical properties, is also verified to be significantly superior to its counterparts in protecting the Al foil from corrosion.[7,14,15] This magic power of $LiPF_6$ is generally attributed to the additional formation of AlF_3 on top of oxide layer in the early cycles with the participation of F^-, originating from the unavoidable thermal decomposition of $LiPF_6$ and its ready reaction with trace amount of H_2O in the electrolyte.[9,14,16] The insoluble AlF_3 could improve the anticorrosion abilities of Al foil by efficiently passivating further solvation/coordination attacked by the anion and solvent molecules. Nonetheless, considering the tenuous thickness of AlF_3 (≈1 nm)[16,17] and accidental inhomogeneities of local current density,[5] the Al foil in the $LiPF_6$-based electrolyte is still subjected to pits corrosion during long-term operations attributed to the accidental breakdown of the protective layers.[6,18] Reasonably, this situation could be further exacerbated by the use of high-voltage positive electrode materials, such as $LiNi_{0.5}Mn_{1.5}O_4$, $LiCoPO_4$, etc.[19]

Compared with $LiPF_6$, imide-based electrolytes like lithium bis(trifluoromethanesulphonyl) imide (LiTFSI), lithium bis(fluorosulfonyl) imide (LiFSI), etc., turn out to be much more corrosive to Al foil.[7,8,14,15] The reason is self-evident: imides are much more stable than $LiPF_6$, so no passive films like AlF_3 could form.[13,20] Recently, superconcentrated imide electrolyte was demonstrated to be efficacious in inhibiting the corrosion of Al foil.[13,19,21,22] The plausible reason is that owing to the dramatically reduced numbers of free anions or solvent molecules in superconcentrated electrolyte, both the formation of Al-complexes and desorption of Al-complexes are inhibited consequently. Such exciting findings are indeed scientifically enlightening, yet seem technologically nonviable in light of the compromised lithium-ion conductivity as well as the significantly elevated cost. Other dedicated efforts, such as developing additives,[20] fine-tailoring the anion size[4,23] and the solvent compositions,[24] and so on, have achieved limited success.

Clearly, whatever electrolyte systems are, the corrosion of Al foil as current collector is still a haunting issue plaguing the long-term performance and reducing the service life of LIBs. For the deployment of 5 V LIBs in the future, which is imperative among the battery community to increase the energy density, the case would be further exacerbated.[1]

Here, we use graphene film, a 2D layered semimetal which is impermeable to species except proton,[25] as electrically conductive coating layers and interfacial barrier layers to enhance the anticorrosion performances of Al foil. In detail, the multilayer graphene (MLG) films, which are directly and conformally grown on industrial Al foil via plasma-enhanced chemical vapor deposition (PECVD) method, serve as extraordinary conductive shield that could efficiently thwart the attacks of the anions or other coordinating species to Al^{3+}. As a consequence, the possibility of the coordination between Al^{3+} and other species would be drastically minimized or even disabled. And thus, the Al foil armored with conductive graphene sheath shows significantly reinforced resistance against the anodic corrosions (**Figure 1**). Moreover, using $LiMn_2O_4$ as a model system, the cells using graphene-armored Al foil (GA) as current collectors demonstrate enhanced electrochemical performance, including better long-term cycling performance at low rate, relieved self-discharge propensity, and enhanced rate/power performance.

The MLG on Al foil was synthesized via PECVD method. The primary consideration of choosing PECVD method is that it is capable of synthesizing graphene at relatively low temperature, considering the melting point of Al foil (≈660 °C). The growth temperature was set to be 600 °C, which is below the melting point of Al foil (see the Experimental Section for details). This growth condition ensures that compared with pristine Al foil (PA), there are no macroscopic or microscopic morphology changes of GA (**Figure 2**a and Figure S1, Supporting Information). Raman spectrum shows that the as-synthesized graphene films are considerably high-quality despite of the low synthesis temperature (Figure 2b). The X-ray photoelectron spectroscopic (XPS) signal of C 1s shows the dominant sp^2 nature of as-synthesized MLG (Figure 2c). Notably, the relatively high ratio of C–O suggests the efficient bondings between MLG and the native oxide layer, implying the tight adhesion and good electrical contacts of MLG on Al foil. Cross-sectional transmission electron microscopy (TEM) image unambiguously shows no visible gap between MLG and Al foil, which confirms its superiority to the reported transfer methods.[26,27] After the Al foil was etched in dilute HCl solution (aq. 0.05 M), the as-synthesized MLG was carefully transferred onto holey grids without any polymer media for TEM observations to determine the uniformity. TEM observations clearly corroborate that the as-synthesized graphene are uniform film without pinholes, suggesting that Al foil is conformally coated with MLG (Figure 2f). The thickness of graphene films is generally 9–12 layers (growth time was about 7 min, inset of Figure 2f).

To diagnose the anodic corrosion properties of GA, we carried out harsh electrochemical tests of the pristine aluminum foil and graphene-armored aluminum foil. Briefly, 2016-type coin cells were fabricated by using GA (or PA) as positive electrode and lithium foil as counter/reference electrode (i.e., GA(or PA)/electrolyte/Li) for cyclic voltammetry (CV), chronoamperometry (CA) examinations. To exclude the influence of the electrolyte dose, 30 µL electrolyte (1 M $LiPF_6$ or LiTFSI) was standardly added for each cell.

For the first cycle of CV, the anodic current of GA is comparable to or slightly lower than that of PA (PA 1) and the upturn

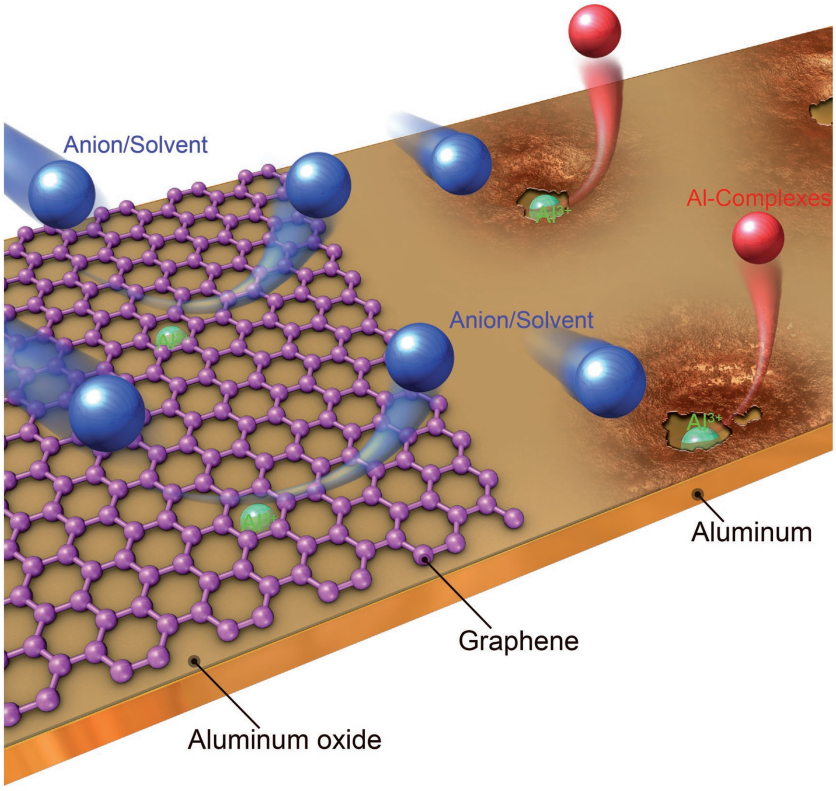

Figure 1. Schematic illustration of graphene-armored aluminum foil with enhanced anticorrosion property as current collectors for LIBs. For the sake of presentation, the sizes of Al^{3+} and the anion/ solvent species are not commensurate with their real species and graphene sheath is simplified into one layer.

inflection voltage (V_{up}) of GA1 (4.08 V vs Li^+/Li) is also slightly higher than that of PA1 (4 V vs Li^+/Li) (**Figure 3**a,b). Furthermore, the anodic current of GA decreased with progressive cycling, which is presumably attributed to the concomitant passivation. Accordingly, the V_{up} is remarkably elevated up to ≈4.5 V (vs Li^+/Li) since the third cycle (Figure 3a). However, the evolution of the CV curves of PA seems sharply contrasted and more complicated (Figure 3b). The anodic current of PA decreased with progressive cycling for the early four cycles, indicative of the passivation of PA like GA. Strikingly, it increases dramatically during the fifth cycle (PA 5). This scenario strongly implies the local breakdown of the protective passive layers, as aforementioned. Moreover, the V_{up} remains nearly unchanged (around 4 V) or even slightly decreased. Then, the Al foils were carefully dissembled from the cells to check the morphology change of GA/PA after CV measurements. Postmortem observations clearly show that GA survived robustly without any appreciable change after five CV cycles (Figure 3c), while PA was seriously corroded with apparent scars (Figure 3d). As previously reported,[26] quantitative XPS examinations confirm that the amount of F on the GA after CV was far less than that on the PA, which in turn reflects that the production of

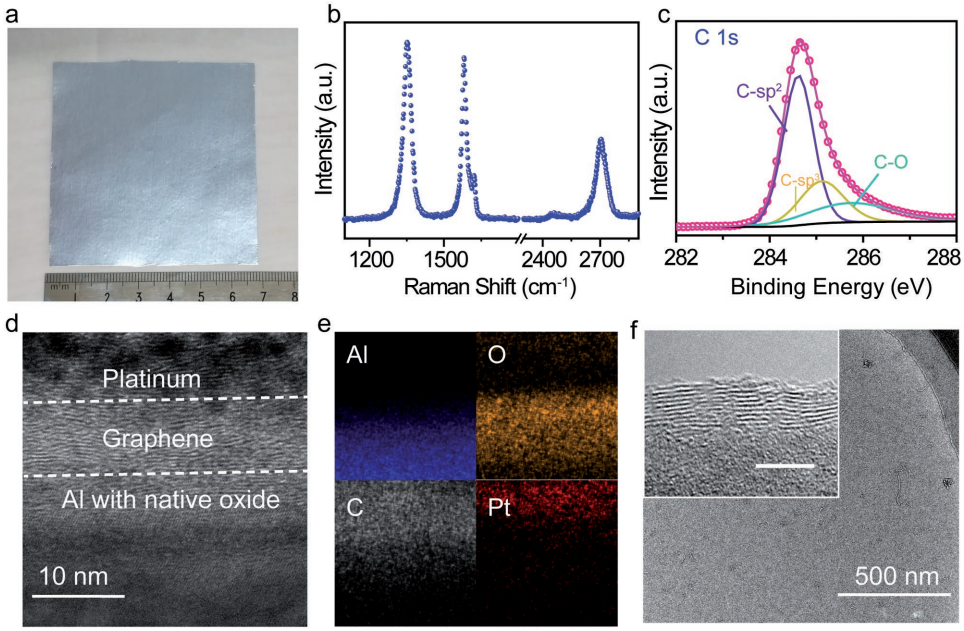

Figure 2. Synthesis and characterization of graphene-armored Al foil via PECVD. a) Digital camera image of as-synthesized GA. b) Typical Raman spectrum of GA. c) XPS signal of C 1s of GA. d,e) High-resolution cross-sectional transmission electron microscopy (TEM) image and corresponding elemental mapping of GA. Platinum was thermally deposited to protect graphene from possible damage during sampling. f) Low-magnification TEM image of as-synthesized multilayer graphene (MLG). Inset is high-resolution TEM image of MLG. Scale bar: 5 nm.

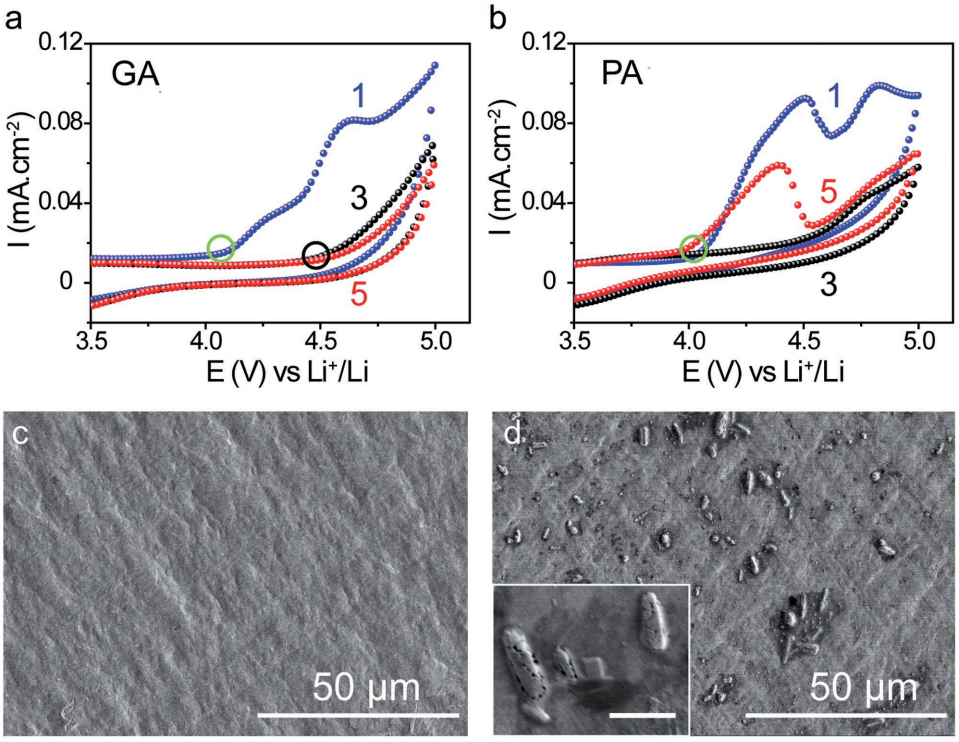

Figure 3. Enhanced anticorrosion performance of GA. a,b) CV curves of GA and PA in LPF_6 electrolyte, respectively. The number denotes the cycle index. c,d) SEM images of GA and PA after CV examinations, respectively. The scale bar of the inset in (d) is 2 μm.

Al^{3+} from GA could be drastically inhibited (Figure S2a, Supporting Information). Logically, this means that in comparison with PA, the corrosion degree of GA is drastically inhibited.

For CA analyses, PA and GA were anodically polarized to 4.2 V for 1 h. Similar to the results of CV examinations, GA shows no perceptible morphology change (Figure S3a, Supporting Information). However, the PA was strikingly corroded into patterns, which are somewhat reminiscent of the anodic alumina oxide templates (Figure S3b, Supporting Information).[28] Likewise, XPS examinations also confirm the dramatically inhibited corrosion degree of GA (Figure S2b, Supporting Information).

We further examine the anticorrosion performances of GA in the more corrosive imide-based electrolyte likewise. Our preliminary result suggests that GA is also resistant against the corrosions in LiTFSI-based electrolyte (Figure S4, Supporting Information).

Briefly, our systematic analyses unambiguously indicate the strong and robust anticorrosion performances of Al foil armored by graphene in both the $LiPF_6$-based and LiTFSI-based electrolyte. Remarkably, extensive Raman characterizations of the GA after both CV and CA examinations show no appreciable changes as compared with the freshly synthesized GA (Figure S5, Supporting Information), further confirming the excellent robustness and good adhesion of MLG on graphene.

To examine the performance of GA as current collectors for LIBs, $LiMn_2O_4$ (Figure S6, Supporting Information) was used as a model material system of positive electrode. Coin cells were assembled in half cell configuration where lithium foil serves as reference/counter electrode. Generally, the influence of current collector to the cell performance is usually delicate. To fairly and reliably compare the role of current collectors, we carefully assembled $LiMn_2O_4$ cells with same mass of the loaded active materials and electrode thickness for critical studies.

The cycling performance at low-rate of charging and discharging can be divided in to three regions: early stage I, middle stage II, and long-term stage III (**Figure 4**a). During stage I, the performances of LMO/PA and LMO/GA are nearly the same, including the cycling trend. For example, during the first cycle, the specific capacities of charging/discharging are 106/101 mAh g^{-1} for LMO/PA and 107/100 mAh g^{-1} for LMO/GA, respectively. In stage II, LMO/PA shows slightly better performance than that of LMO/GA. However, the superiority of LMO/GA is rather prominent in terms of long-term cycling (stage III), which shows a much slower capacity fading. In detail, after ≈950 h straight operations at 0.5 C, the discharge capacity retention (DCR) of LMO/GA reaches up to 91%, which is remarkably superior to LMO/PA cell (DCR is 75%).

Undoubtedly, the decay of LMO/GA cell should be first attributed to the intrinsic electrochemical characteristics of LMO itself during charge and discharge, e.g., the John–Teller effect, the dissolution of Mn, etc.[29,30] But the corrosions of current collector (and related parasitic side reactions) also play a part, in view of the anatomy results showing that PA suffered from far more serious corrosions than GA after cycling (Figure S7, Supporting Information). The results validate: i) our unbiased efforts of extracting the effect of graphene-armored Al foil as current collectors, as confirmed by the cell performances in early stage; ii) the corrosion of current collector is indeed

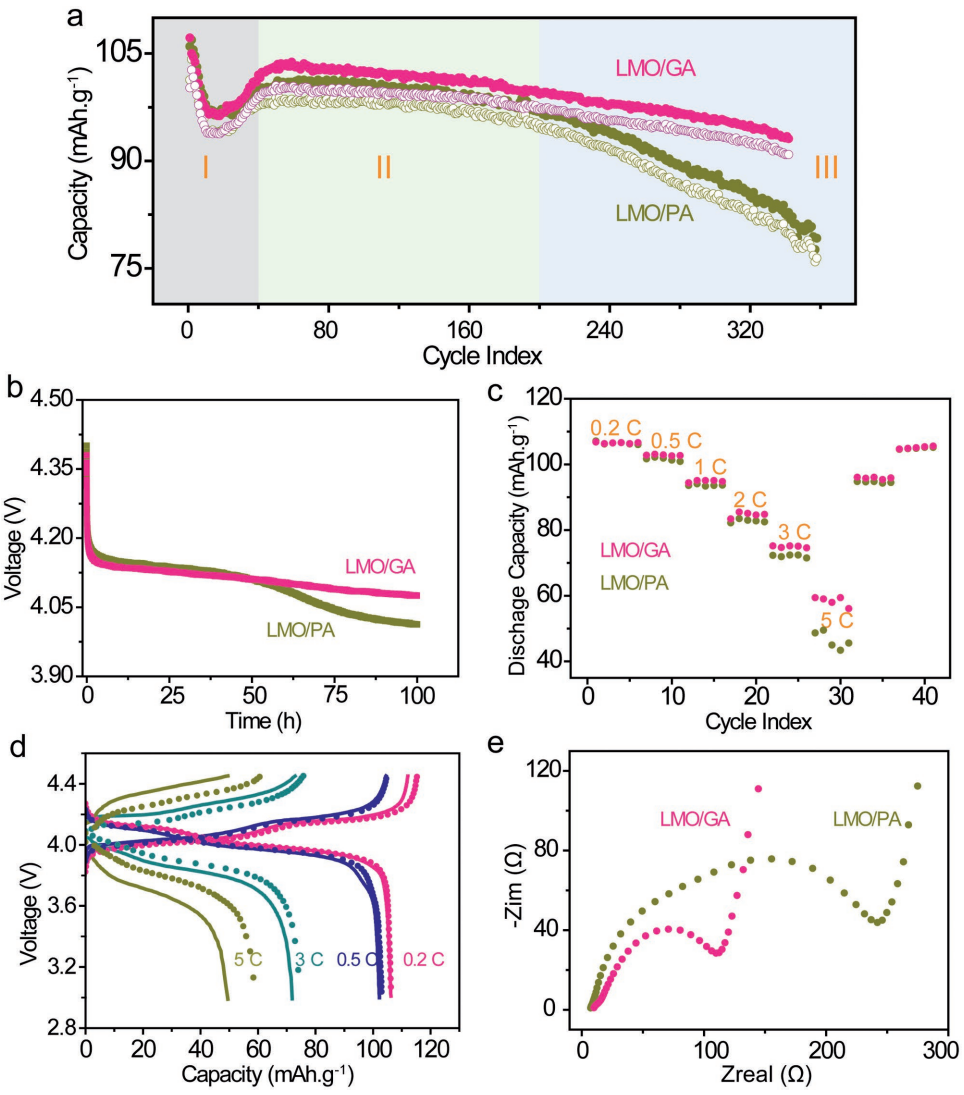

Figure 4. Enhanced electrochemical performance of GA. a) Long-term low-rate (0.5 C, 1C = 148 mA g^{-1}) cycling performance of LMO/PA and LMO/GA cells. Solid and circle represent the C_{cha} and C_{dis}, respectively. b) Self-discharging properties of LMO/PA and LMO/GA cells. c,d) Rate/power performances of LMO/PA and LMO/GA cells and corresponding charge/discharge curves, respectively. Solid line and circle represent the LMO/PA and LMO/GA cells, respectively. e) EIS analysis of LMO/PA and LMO/GA cells.

an important factor affecting the long-term performance; and iii) the unambiguous advantage of using GA as current collectors in terms of long-term performance in spite of low rate operation, as confirmed by the middle and late stages.

Besides, the self-discharge property is also a significant dimension of LIBs. Previous works established that it is closely associated with the corrosion of current collectors.[31] In light of the dramatically improved anticorrosion properties of GA, we compared the self-discharge performance of LMO/PA and LMO/GA cells. The self-discharge of LMO/GA cell is significantly relieved in the long term (Figure 4b and Figure S8a, Supporting Information). Similarly, GA seemed to suffer from much less serious corrosions after the self-discharge tests (Figure S8b,c, Supporting Information).

The rate tests show that their performances are not quite distinguishable at low rate, similar to stage I in the cycling performance. However, LMO/GA has superior rate/power performance (Figure 4c). The charge/discharge curves unveil that the polarization of LMO/GA is much smaller than that of its LMO/PA counterpart in the high current density regime (Figure 4d). Electrochemical impedance spectroscopy (EIS) diagnosis further corroborates that the enhanced kinetics arose from the reduced charge transfer resistance with the mediation of graphene (Figure 4e). We note that similar result has been reported for negative electrode, which shows that graphene modified copper as current collectors would enhance rate/power performance.[32] In addition, there are other latent advantages for the graphene armored current collectors. For instance, the adhesion between the current collector and active materials would be tighter and closer, and the thermal dissipation would be promoted considering the extraordinary thermal conductivity,[33] as demonstrated in the recently released battery technologies with graphene.[34]

To sum up, by taking advantage of the impenetrable signature of graphene, we use graphene sheath to armor the Al

foil to reinforce its anti-anodic corrosion property in both the $LiPF_6$-and imide-based electrolytes. More importantly, our critical studies clearly show that $LiMn_2O_4$ cells using graphene-armored Al foil as current collectors would demonstrate superior electrochemical performance, including better long-term cycling as well as rate performance and significantly ameliorated self-discharging property. Given the imperative among the battery community to elevate the voltage of LIBs from the present 4 V to 5 V in the future to increase the energy density, the corrosions of Al foil would be reasonably more highlighted. Ongoing efforts are dedicated to testing the performance of graphene-armored Al foil as current collectors for 5 V LIBs in our laboratory. Finally, given the impressive progress achieved in the mass-production of graphene,[35–37] we strongly believe our method holds envious promise for the amelioration of the long-term stable operation of LIBs. Our work might open another promising avenue toward the killer application of graphene and foster a niche market of this superstar material.[38–41]

Experimental Section

MLG Synthesis via PECVD: The plasma generator was made up of Cu coil and RF power (RFG-500 RF Power, Tailong Electronics). In a typical procedure, commercially available Al foil (battery grade, ≈15 µm, Shenzhen Kejing Star Technology Co., LTD) was placed in the hot center of the furnace, with a distance of 25 cm between the sample center and the Cu coil center. After being evacuated to base pressure of 0.1 Pa and purged with argon for several times, the system was initially heated to 600 °C in 20 min with 100 standard-state cubic centimeter per minute (sccm) hydrogen. Afterward, 7 sccm methane was introduced in the system with a pressure of ≈15 Pa and plasma generator was turned on with a power of 150 W to generate methane plasma. The deposition lasted for 5–10 min, followed by rapid cooling process to room temperature.

Battery Electrochemistry: For anticorrosion examinations, 2016 type coin cells were assembled using PA (GA) as working electrode and lithium foil as counter/reference electrode in glove box (O_2 < 0.5 ppm, H_2O < 0.5 ppm). 30 µL electrolyte (1 M $LiPF_6$, ethylene carbonate(EC):dimethyl carbonate(DMC) = 50:50 vol%, purchased from Zhangjiagang Guotai Huarong Chemical New Material Co., Ltd and used as received) was standardly added for each cell. CV analyses were carried out in the range of 2–5 V (vs Li^+/Li) with scanning speed of 10 mV s^{-1}. The voltage of CA analyses was 4.2 V (vs Li^+/Li) with duration of 1 h. After the CV or CA analyses, coin cells were carefully dissembled to take PA (GA) electrodes out and thoroughly washed with DMC for subsequent morphology examinations. Both CV and CA tests were performed on Biologic VMP3.

To examine the electrochemical performances of $LiMn_2O_4$ cells, the $LiMnO_4$ half cells were assembled following conventional practices. Briefly, $LiMn_2O_4$ powders (Alfa Aesar, 99.5% metal basis) and conducting additives (super P) and polyvinylidene difluoride (PVDF) were thoroughly mixed with 1-methyl-2-pyrrolidinone (NMP) in the ratio of 90:5:5 to get the slurry. Then the slurry was cast onto the current collectors (PA and GA). And the electrodes were sequentially dried in air oven at 80 °C for 200 min and vacuum oven at 110 °C for 6 h. Finally, the electrodes were cut into 1 cm disks and assembled into 2016 type coin cells using lithium foil as counter/reference electrode. 30 µL electrolyte (1 M $LiPF_6$, EC:DMC = 50:50 vol%) was standardly added for each cell. For a fair comparison, the mass of the loaded active material was controlled ≈6 mg cm^{-2} and the overall thickness after rolling was ≈52 µm. The cells were aged for 6 h before electrochemical tests. Galvanostatic cycling was conducted on the LAND battery tester. For the self-discharge tests, the cells were charged to 4.5 V at the rate of 0.3 C, and then the voltage of the cells was monitored. The electrochemical impedance spectroscopy measurements were carried out on a Biologic VMP3 system with an excitation of 5 mV (frequency range: 500 kHz–10 mHz).

Characterization: Scanning electron microscopy was conducted on Hitachi S-4800 (acceleration voltage 0.5–5 kV) and atomic force microscopy was performed on Bruker Dimension Icon in tapping mode. Raman spectra were collected on a Horiba HR800 Raman system using 514 nm laser for excitation. The cross-sectional TEM sample was prepared by using a focused ion beam system (FIB, FET Strata DB 235). The TEM images and elemental mapping (energy dispersive X-ray spectra) were acquired in an aberration-corrected FEI microscope (Titan Cubed Themis G2) operated at 80 kV.

Supporting Information

Supporting Information is available from the Wiley Online Library or from the author.

Acknowledgements

This work was financially supported by Beijing Municipal Science & Technology Commission (Nos. Z161100002116002 and Z161100002116021), the National Basic Research Program of China (Nos. 2014CB932500 and 2016YFA0200101), the National Natural Science Foundation of China (Nos. 21525310, 51432002, 51502007, and 51520105003), and National Program for Support of Top-Notch Young Professionals.

Conflict of Interest

The authors declare no conflict of interest.

Keywords

aluminum foil, anti-corrosion, current collectors, graphene, lithium-ion batteries

Received: July 12, 2017
Revised: August 18, 2017
Published online: October 27, 2017

[1] J. B. Goodenough, K.-S. Park, *J. Am. Chem. Soc.* **2013**, *135*, 1167.
[2] J. B. Goodenough, *Acc. Chem. Res.* **2013**, *46*, 1053.
[3] S.-T. Myung, Y. Hitoshi, Y.-K. Sun, *J. Mater. Chem.* **2011**, *21*, 9891.
[4] L. J. Krause, W. Lamanna, J. Summerfield, M. Engle, G. Korba, R. Loch, R. Atanasoski, *J. Power Sources* **1997**, *68*, 320.
[5] Y. F. Chen, T. M. Devine, J. W. Evans, O. R. Monteiro, I. G. Brown, *J. Electrochem. Soc.* **1999**, *146*, 1310.
[6] X. Y. Zhang, B. Winget, M. Doeff, J. W. Evans, T. M. Devine, *J. Electrochem. Soc.* **2005**, *152*, B448.
[7] S. S. Zhang, T. R. Jow, *J. Power Sources* **2002**, *109*, 458.
[8] H. Yang, K. Kwon, T. M. Devine, J. W. Evans, *J. Electrochem. Soc.* **2000**, *147*, 4399.
[9] T. C. Hyams, J. Go, T. M. Devine, *J. Electrochem. Soc.* **2007**, *154*, C390.
[10] J. Wen, Y. Yu, C. Chen, *Mater. Express* **2012**, *2*, 197.
[11] X. Zhang, P. N. Ross, R. Kostecki, F. Kong, S. Sloop, J. B. Kerr, K. Striebel, E. J. Cairns, F. McLarnon, *J. Electrochem. Soc.* **2001**, *148*, A463.
[12] X. M. Wang, E. Yasukawa, S. Mori, *Electrochim. Acta* **2000**, *45*, 2677.
[13] Y. Yamada, C. H. Chiang, K. Sodeyama, J. Wang, Y. Tateyama, A. Yamada, *Chemelectrochem* **2015**, *2*, 1687.

[14] K. Kanamura, T. Okagawa, Z. Takehara, *J. Power Sources* **1995**, *57*, 119.
[15] M. Morita, T. Shibata, N. Yoshimoto, M. Ishikawa, *Electrochim. Acta* **2002**, *47*, 2787.
[16] X. Zhang, T. M. Devine, *J. Electrochem. Soc.* **2006**, *153*, B344.
[17] M. Martin, E. Fromm, *Thin Solid Films* **1993**, *236*, 199.
[18] B. C. Bunker, G. C. Nelson, K. R. Zavadil, J. C. Barbour, F. D. Wall, J. P. Sullivan, C. F. Windisch, M. H. Engelhardt, D. R. Baer, *J. Phys. Chem. B* **2002**, *106*, 4705.
[19] J. Wang, Y. Yamada, K. Sodeyama, C. H. Chiang, Y. Tateyama, A. Yamada, *Nat. Commun.* **2016**, *7*, 12032.
[20] W. K. Behl, E. J. Plichta, *J. Power Sources* **1998**, *72*, 132.
[21] K. Matsumoto, K. Inoue, K. Nakahara, R. Yuge, T. Noguchi, K. Utsugi, *J. Power Sources* **2013**, *231*, 234.
[22] D. W. McOwen, D. M. Seo, O. Borodin, J. Vatamanu, P. D. Boyle, W. A. Henderson, *Energy Environ. Sci.* **2014**, *7*, 416.
[23] H. Han, J. Guo, D. Zhang, S. Feng, W. Feng, J. Nie, Z. Zhou, *Electrochem. Commun.* **2011**, *13*, 265.
[24] X. M. Wang, E. Yasukawa, S. Mori, *J. Electrochem. Soc.* **1999**, *146*, 3992.
[25] S. Hu, M. Lozada-Hidalgo, F. C. Wang, A. Mishchenko, F. Schedin, R. R. Nair, E. W. Hill, D. W. Boukhvalov, M. I. Katsnelson, R. A. W. Dryfe, I. V. Grigorieva, H. A. Wu, A. K. Geim, *Nature* **2014**, *516*, 227.
[26] S. J. R. Prabakar, Y.-H. Hwang, E. G. Bae, D. K. Lee, M. Pyo, *Carbon* **2013**, *52*, 128.
[27] X. Zhao, Y.-M. Lin, *US 20140030636A1*, **2014**.
[28] W. Lee, S.-J. Park, *Chem. Rev.* **2014**, *114*, 7487.
[29] B. L. Ellis, K. T. Lee, L. F. Nazar, *Chem. Mater.* **2010**, *22*, 691.
[30] P. Gao, R. Ishikawa, E. Tochigi, A. Kumamoto, N. Shibata, Y. Ikuhara, *Chem. Mater.* **2017**, *29*, 1006.
[31] S. S. Zhang, M. S. Ding, T. R. Jow, *J. Power Sources* **2001**, *102*, 16.
[32] J. Jiang, P. Nie, B. Ding, W. Wu, Z. Chang, Y. Wu, H. Dou, X. Zhang, *ACS Appl. Mater. Interfaces* **2016**, *8*, 30926.
[33] A. A. Balandin, *Nat. Mater.* **2011**, *10*, 569.
[34] http://www.huawei.com/cn/news/2016/12/Graphene-Assisted-Li-ion-Batteries.
[35] S. Bae, H. Kim, Y. Lee, X. Xu, J.-S. Park, Y. Zheng, J. Balakrishnan, T. Lei, H. R. Kim, Y. I. Song, Y.-J. Kim, K. S. Kim, B. Ozyilmaz, J.-H. Ahn, B. H. Hong, S. Iijima, *Nat. Nanotechnol.* **2010**, *5*, 574.
[36] B. Deng, P.-C. Hsu, G. Chen, B. N. Chandrashekar, L. Liao, Z. Ayitimuda, J. Wu, Y. Guo, L. Lin, Y. Zhou, M. Aisijiang, Q. Xie, Y. Cui, Z. Liu, H. Peng, *Nano Lett.* **2015**, *15*, 4206.
[37] L. F. Cui, X. P. Wang, N. Chen, G. F. Zhang, L. T. Qu, *J. Mater. Chem. A* **2017**, *5*, 14508.
[38] R. Raccichini, A. Varzi, S. Passerini, B. Scrosati, *Nat. Mater.* **2015**, *14*, 271.
[39] A. K. Geim, K. S. Novoselov, *Nat. Mater.* **2007**, *6*, 183.
[40] L. Ji, P. Meduri, V. Agubra, X. Xiao, M. Alcoutlabi, *Adv. Energy Mater.* **2016**, *6*, 1502159.
[41] Y. Dong, Z.-S. Wu, W. Ren, H.-M. Cheng, X. Bao, *Sci. Bull.* **2017**, *62*, 724.